Cellular/Molecular

Miniature IPSCs in Hippocampal Granule Cells Are Triggered by Voltage-Gated Ca^{2+} Channels via Microdomain Coupling

Sarit Pati Goswami,[1,2] Iancu Bucurenciu,[3]* and Peter Jonas[1]*

[1]IST Austria (Institute of Science and Technology Austria), A-3400 Klosterneuburg, Austria, [2]Spemann Graduate School of Biology and Medicine (SGBM) and Faculty of Biology, University of Freiburg, D-79104 Freiburg, Germany, and [3]Epilepsiezentrum Kork, D-77694 Kehl-Kork, Germany

The coupling between presynaptic Ca^{2+} channels and Ca^{2+} sensors of exocytosis is a key determinant of synaptic transmission. Evoked release from parvalbumin (PV)-expressing interneurons is triggered by nanodomain coupling of P/Q-type Ca^{2+} channels, whereas release from cholecystokinin (CCK)-containing interneurons is generated by microdomain coupling of N-type channels. Nanodomain coupling has several functional advantages, including speed and efficacy of transmission. One potential disadvantage is that stochastic opening of presynaptic Ca^{2+} channels may trigger spontaneous transmitter release. We addressed this possibility in rat hippocampal granule cells, which receive converging inputs from different inhibitory sources. Both reduction of extracellular Ca^{2+} concentration and the unselective Ca^{2+} channel blocker Cd^{2+} reduced the frequency of miniature IPSCs (mIPSCs) in granule cells by ~50%, suggesting that the opening of presynaptic Ca^{2+} channels contributes to spontaneous release. Application of the selective P/Q-type Ca^{2+} channel blocker ω-agatoxin IVa had no detectable effects, whereas both the N-type blocker ω-conotoxin GVIa and the L-type blocker nimodipine reduced mIPSC frequency. Furthermore, both the fast Ca^{2+} chelator BAPTA-AM and the slow chelator EGTA-AM reduced the mIPSC frequency, suggesting that Ca^{2+}-dependent spontaneous release is triggered by microdomain rather than nanodomain coupling. The CB_1 receptor agonist WIN 55212-2 also decreased spontaneous release; this effect was occluded by prior application of ω-conotoxin GVIa, suggesting that a major fraction of Ca^{2+}-dependent spontaneous release was generated at the terminals of CCK-expressing interneurons. Tonic inhibition generated by spontaneous opening of presynaptic N- and L-type Ca^{2+} channels may be important for hippocampal information processing.

Introduction

The physical distance between presynaptic Ca^{2+} channels and Ca^{2+} sensors of exocytosis is a key determinant of efficacy and speed of synaptic transmission (Neher and Sakaba, 2008; Eggermann et al., 2012). The tightness of the coupling has several implications for the functional properties of evoked transmitter release. Nanodomain coupling between Ca^{2+} channels and Ca^{2+} sensors of exocytosis (i.e., coupling with a distance of $<$100 nm) (Eggermann et al., 2012) increases the release probability, reduces the synaptic delay, and sharpens the time course of quantal release (Bucurenciu et al., 2008; Christie et al., 2011). In contrast, microdomain coupling (i.e., coupling with a distance $>$100 nm) may enable presynaptic forms of synaptic plasticity (Ahmed and Siegelbaum, 2009), for example by modulatory control via intracellular Ca^{2+} buffers.

The coupling configuration also has major implications for spontaneous release (Stanley, 1997; Eggermann et al., 2012). One potential disadvantage of nanodomain coupling is that stochastic openings of presynaptic Ca^{2+} channels may trigger spontaneous transmitter release events, which will be reflected by a high frequency of miniature synaptic events (Stanley, 1997; Ribrault et al., 2011). However, this hypothesis has not been directly tested. Moreover, the mechanisms of spontaneous release at central synapses have remained highly controversial. While in some synapses spontaneous release is independent of Ca^{2+} inflow and external or internal Ca^{2+} concentration (Scanziani et al., 1992; Llano and Gerschenfeld, 1993), in several other synapses the Ca^{2+} dependence is well documented (Hoffman and Lupica, 2000; Llano et al., 2000; Angleson and Betz, 2001; Lou et al., 2005; Vyleta and Smith, 2011). Whether miniature synaptic events are driven by spontaneous Ca^{2+} channel opening, as predicted in tight coupling regimes, however, has remained unclear.

Spontaneous Ca^{2+} channel openings could drive spontaneous transmitter release in different ways. In a nanodomain coupling regime, single Ca^{2+} channel openings would lead to brief and local rises in Ca^{2+} concentration, directly triggering the fusion of synaptic vesicles. In a microdomain coupling configura-

Received Dec. 7, 2011; revised Aug. 7, 2012; accepted Aug. 15, 2012.

Author contributions: I.B. and P.J. designed research; S.P.G. performed research; S.P.G. and P.J. analyzed data; I.B. and P.J. wrote the paper.

This work was supported by grants from the Deutsche Forschungsgemeinschaft (TR 3/B10, Leibniz program, GSC-4 Spemann Graduate School) and the European Union (European Research Council Advanced Grant). We thank Drs. José Guzmán, Alejandro Pernía-Andrade, and Nicholas Vyleta for reading earlier versions of this manuscript.

*These authors contributed equally to this work and both serve as corresponding authors.

Correspondence should be addressed to either of the following: Dr. Peter Jonas, IST Austria (Institute of Science and Technology Austria), Am Campus 1, A-3400 Klosterneuburg, Austria, E-mail: peter.jonas@ist.ac.at; or Dr. Iancu Bucurenciu, Epilepsiezentrum, Kork, Landstrasse 1, D-77694 Kehl-Kork, Germany. E-mail: ibucurenciu@epilepsiezentrum.de.

DOI:10.1523/JNEUROSCI.6104-11.2012

 0270-6474/12/3214294-11$15.00/0

Table 1. Effects of different experimental manipulations on mIPSC frequency and amplitude in hippocampal granule cells

Experimental condition	Frequency (% of control) Mean ± SEM	*p*	Amplitude (% of control) Mean ± SEM	*p*	*n*
Ca^{2+} (0.2 mM)	53.1 ± 8.4	$p < 0.05$	93.1 ± 5.5	$p > 0.1$	6
Cd^{2+} (200 μM)	53.5 ± 5.3	$p < 0.05$	79.9 ± 7.0	$p > 0.05$	6
Cd^{2+} (200 μM) at 32°C	55.1 ± 10.1	$p < 0.05$	84.8 ± 6.6	$p > 0.05$	5
KCl (0.5 mM)	56.7 ± 5.9	$p < 0.05$	98.6 ± 5.0	$p > 0.1$	8
KCl (20 mM)	360.7 ± 70.1	$p < 0.05$	119.8 ± 12.9	$p > 0.1$	6
KCl (0.5 mM) + Cd^{2+} (200 μM)	109.3 ± 12.6	$p > 0.1$	90.7 ± 7.4	$p > 0.1$	5
KCl (20 mM) + Cd^{2+} (200 μM)	42.9 ± 5.0	$p < 0.05$	78.6 ± 4.5	$p = 0.05$	6
ω-Agatoxin IVa (1 μM)	101.4 ± 9.1	$p > 0.1$	93.0 ± 4.9	$p > 0.1$	7
ω-Conotoxin GVIa (1 μM)	77.0 ± 5.9	$p < 0.05$	100.8 ± 4.0	$p > 0.1$	10
Nimodipine (20 μM)	79.1 ± 4.0	$p < 0.05$	103.5 ± 2.5	$p > 0.1$	5
Nimodipine (20 μM) + ω-conotoxin GVIa (1 μM)	101.9 ± 5.8	$p > 0.1$	92.2 ± 3.1	$p > 0.1$	10
Bay K 8644 (20 μM)	128.5 ± 10.2	$p < 0.05$	98.2 ± 5.8	$p > 0.1$	7
NNC 55-0396 (10 μM)	105.9 ± 11.6	$p > 0.1$	107.1 ± 2.3	$p > 0.1$	5
SNX-482 (500 nM)	98.7 ± 2.3	$p > 0.1$	94.7 ± 3.8	$p > 0.1$	5
WIN 55212-2 (3 μM)	74.9 ± 4.3	$p < 0.05$	106.6 ± 1.2	$p > 0.1$	6
ω-Conotoxin GVIa (1 μM) + WIN 55212-2 (3 μM)	101.9 ± 10.2	$p > 0.1$	97.4 ± 5.5	$p > 0.1$	6
BAPTA-AM (100 μM)	56.8 ± 3.4	$p < 0.05$	95.2 ± 5.3	$p > 0.1$	5
EGTA-AM (100 μM)	60.9 ± 6.5	$p < 0.05$	105.1 ± 5.6	$p > 0.1$	5

Effects of experimental manipulations were quantified close to steady-state conditions, i.e. between 10 and 30 min after the onset of the solution change. All mIPSC frequency and amplitude values were compared with corresponding prior control data, with the exception of the experiments with 0.5 and 20 mM KCl + Cd^{2+}, which were compared with 0.5 and 20 mM KCl, those with ω-conotoxin GVIa + WIN 55212-2, which were compared with ω-conotoxin GVIa, and those with nimodipine + ω-conotoxin GVIa, which were compared with nimodipine. The amplitude distribution in 20 mM KCl is shifted to larger values, probably consistent with compound transmitter release (Llano et al., 2000; He et al., 2009). Furthermore, the amplitude distribution in Cd^{2+} is shifted to smaller values. This would be consistent with either reduction of compound transmitter release or direct block of postsynaptic $GABA_A$ receptors (Kaneko and Tachibana, 1986; Mayer and Vyklicky, 1989).

tion, however, multiple Ca^{2+} channel openings would lead to a long lasting and global rise in Ca^{2+} concentration, which would trigger release tonically. Alternatively, spontaneous release may be exclusively driven by the basal Ca^{2+} concentration in presynaptic terminals. Application of Ca^{2+} chelators with different Ca^{2+} binding rates should help to distinguish between these possibilities. In nanodomain coupling configurations, only fast Ca^{2+} chelators should inhibit release. In microdomain configurations, both fast and slow chelators should be effective. Finally, in a regime where resting Ca^{2+} is relevant, release under steady-state conditions should depend on Ca^{2+} influx and efflux rates, but not on exogenous buffer concentration (Denker et al., 2011; for review, see Neher, 1998).

To address this question, we recorded mIPSCs in dentate gyrus granule cells, the input neurons of the hippocampal formation. Our results identify a new form of tonic inhibition in the dentate gyrus (Farrant and Nusser, 2005), driven by the spontaneous opening of presynaptic N- and L-type Ca^{2+} channels and by spatially extended Ca^{2+} concentration changes. Parts of the results have been published in abstract form (Goswami et al., 2011).

Materials and Methods

Patch-clamp recording from dentate gyrus granule cells in hippocampal slices. Transverse hippocampal slices (300 μm thickness) were cut from the brains of 18- to 21-d-old Wistar rats of either sex using a Leica VT1200 vibratome (Leica Microsystems). Animals were decapitated without anesthesia, in accordance with national and institutional guidelines. Experiments were performed under visual control using infrared differential interference contrast videomicroscopy. Neurons chosen for recording had morphological properties of mature granule cells. Voltage-clamp recordings were made with an Axopatch 200A amplifier (Molecular Devices). Patch pipettes were pulled from thick-walled borosilicate glass tubing. When filled with internal solution, the resistance was 2–3 MΩ. Series resistance (R_s) was 6–10 MΩ; R_s was not compensated, but carefully monitored during the experiments. Recordings were discarded if the R_s changed by >15%. Signals were low-pass filtered at 5 kHz (low-pass Bessel filter) and sampled at 10 kHz. Data acquisition was performed using the program FPulse (U. Fröbe, University of Freiburg, Freiburg, Germany) running under Igor Pro 5.05 on a PC, in conjunction with a 1401plus interface (CED). The holding potential was set to −80 mV in all experiments. Cells with a holding current larger than −130 pA were discarded. The recording temperature was 21–24°C, unless stated differently (i.e., in a subset of Cd^{2+} experiments; Table 1).

Recording and analysis of mIPSCs and mEPSCs. mIPSCs in dentate gyrus granule cells were recorded in the whole-cell configuration in the presence of 1 μM tetrodotoxin (TTX), 10 μM 6-cyano-7-nitroquinoxaline-2,3-dione (CNQX), and 20 μM D-2-amino-5-phosphonopentanoic acid (D-AP5). mEPSCs were recorded in the presence of 1 μM TTX and 10 μM bicuculline methiodide.

mIPSCs and mEPSCs in dentate gyrus granule cells were analyzed using the program Minidet 1.18 (U. Fröbe), running under Igor 6.11 on a PC, which utilizes a two-pass template fit detection algorithm (Jonas et al., 1993; Clements and Bekkers, 1997; Aponte et al., 2006). Briefly, a template was shifted over a 600 s data section sample point by sample point and events were detected based on predefined criteria for correlation coefficient ($r_{crit} > 0.55$) and peak amplitude ($a_{crit} > 8$ pA for mIPSCs, 5 pA for mEPSCs). All detected events were subsequently validated by the user. For display purposes, traces were digitally low-pass filtered with a Gaussian filter at 1 kHz. For experiments in 20 mM KCl, additional high-pass filtering at 1 Hz was performed. For plots of mIPSC frequency against time, frequency was normalized to the control value in each cell and averaged across cells. Event distributions and traces were taken 10–30 min after solution exchange. Histograms typically contained ~500 events for mIPSCs and ~200 events for mEPSCs.

Solutions and chemicals. The internal solution contained the following (in mM): 110 KCl, 35 K-gluconate, 10 EGTA, 2 $MgCl_2$, 2 Na_2ATP, and 10 HEPES, pH adjusted to 7.2 with KOH. The physiological external solution contained the following (in mM): 125 NaCl, 25 $NaHCO_3$, 2.5 KCl, 1.25 NaH_2PO_4, 2 $CaCl_2$, 1 $MgCl_2$, and 25 glucose (equilibrated with 95% O_2/5% CO_2 gas mixture). In low-Ca^{2+} external solution, $CaCl_2$ was reduced to 0.2 mM and $MgCl_2$ was increased to 2.8 mM. In low-KCl external solution, KCl was reduced to 0.5 mM and NaCl was increased to 127 mM. In high-KCl external solution, KCl was increased to 20 mM and NaCl decreased to 107.5 mM, all other constituents remained the same.

Peptide toxins were applied with a recirculation system (volume ~10 ml, flow 1.5 ml min^{-1}, equilibrated with O_2/CO_2). In these experiments, bovine serum albumin (Sigma-Aldrich) was added at a concentration of 1 mg ml^{-1} to the bath solution before and during the experiment to prevent adsorption of the peptides to surfaces. ω-agatoxin IVa and ω-conotoxin GVIa were from

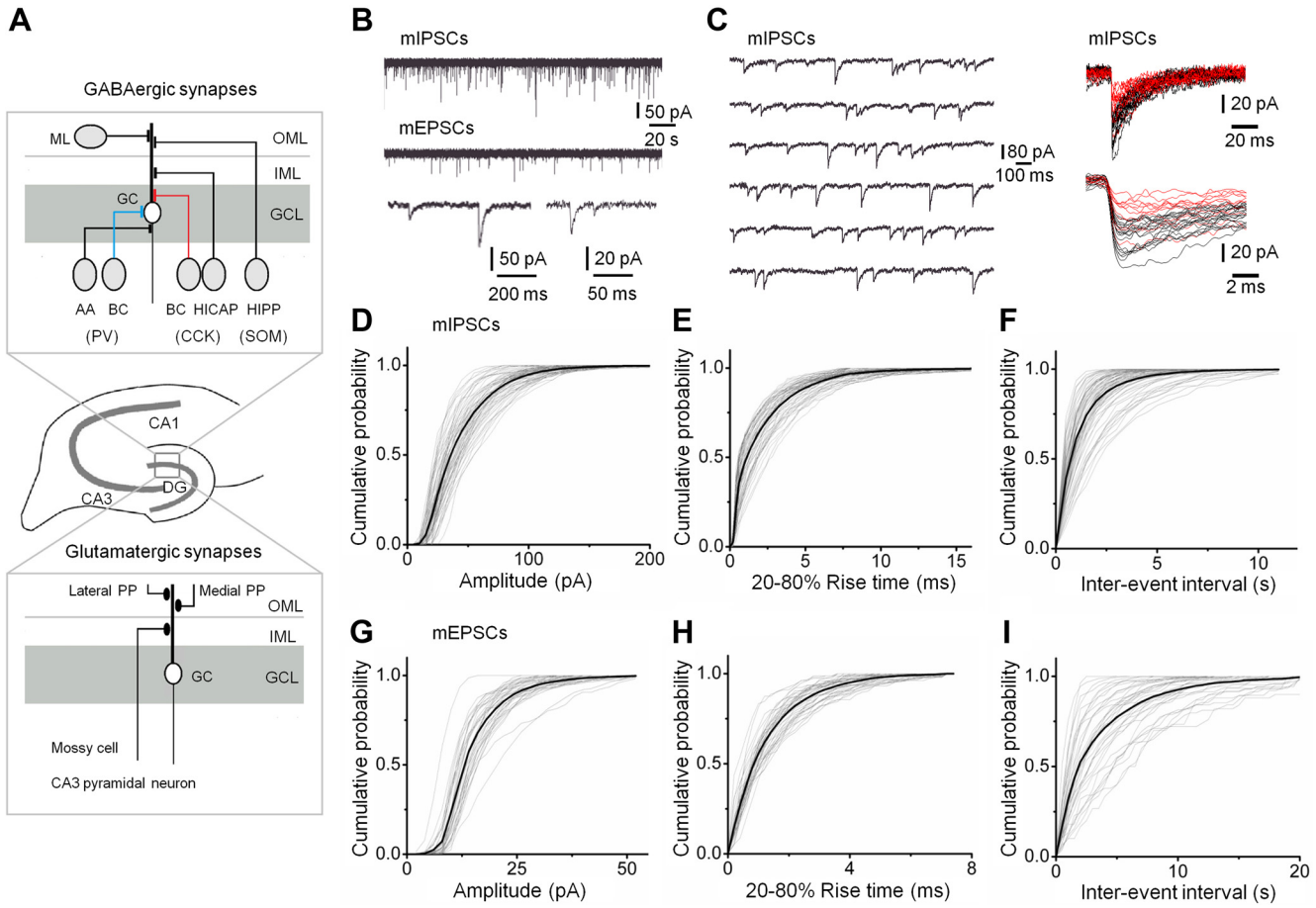

Figure 1. Comparison of miniature IPSCs and EPSCs in hippocampal granule cells. ***A***, Schematic illustration of innervation of dentate gyrus granule cells by different inhibitory and excitatory pathways; AA, axo-axonic cell; BC, basket cell; CCK, cholecystokinin expressing; GC, granule cell; GCL, granule cell layer; HICAP, hilar commissural-associational pathway-related cell; HIPP, hilar perforant path-associated cell; IML, inner molecular layer; ML, molecular layer interneuron; OML, outer molecular layer; PP, perforant path; PV, parvalbumin expressing; SOM, somatostatin expressing; blue axon and red axon represents P/Q- and N- type Ca^{2+} channel gated synaptic transmission, respectively. ***B***, Original traces of mIPSCs and mEPSCs at −80 mV. Top, mIPSCs at compressed time scale; center, mEPSCs at the same scale; bottom, expanded traces for the two types of events. ***C***, Original traces of mIPSCs at expanded time scale. Insets on the right show superpositions of 35 individual events. Events with 20–80% rise times ≥2 ms are indicated in red. Note the variability in peak amplitude and time course, with rapidly rising events likely to be generated at perisomatic sites and slow events at distal dendritic sites. ***D–F***, Peak amplitude (***D***), 20–80% rise time (***E***), and inter-event interval (***F***) distributions of mIPSCs in GCs. Gray lines, Cumulative distributions from individual cells; black lines, average cumulative distribution (66 cells). ***G–I***, Peak amplitude (***G***), 20–80% rise time (***H***), and inter-event interval (***I***) of mEPSCs in GCs. Gray lines, cumulative distributions from individual cells; black lines, average cumulative distribution (37 cells).

Bachem. Ethylene glycol-bis(2-aminoethylether)-*N*,*N*,*N*′,*N*′-tetraacetic acid tetra(acetoxymethyl ester) (EGTA-AM) and 1,2-*bis*(2-aminophenoxy) ethane-*N*,*N*,*N*′,*N*′-tetraacetic acid tetrakis(acetoxymethyl ester) (BAPTA-AM) were from Invitrogen and BioTrend, respectively. BAPTA-AM and EGTA-AM stock solutions were prepared in dimethylsulfoxide (DMSO) and diluted in physiological saline directly before the experiment (final concentration of 0.1% DMSO). SNX-482 and NNC 55-0396 were from Tocris Bioscience, WIN 55212-2, nimodipine and Bay K 8644 were from Sigma-Aldrich. All other chemicals were from Sigma-Aldrich or BioTrend.

Statistical analysis. Values are given as means ± SEMs. Error bars in the figures also indicate SEMs. Significance of differences was assessed by a two-sided nonparametric Wilcoxon signed rank test; differences were considered significant at $p < 0.05$.

Model of stochastic Ca^{2+} channel opening, buffered Ca^{2+} diffusion, and transmitter release. A model of synaptic transmission in which Ca^{2+} channels were coupled to a Ca^{2+} sensor was implemented as follows. First, stepwise openings and closings of a single Ca^{2+} channel at a given membrane potential were simulated, using a Hodgkin–Huxley type Ca^{2+} channel model with two gating particles. As the gating properties of presynaptic P/Q- and N-type Ca^{2+} channels were similar (Li et al., 2007), a uniform gating model was used (Borst and Sakmann, 1998). In a subset of simulations, the voltage dependence of gating was shifted in the range ±10 mV as indicated. The single-channel conductance was assumed as 2.5 pS (Li et al., 2007). Channel openings and closings were simulated as sigmoidal functions with 10 μs steepness. Second, the Ca^{2+} concentration at different distances from the source was calculated by solving the full set of partial differential reaction diffusion equations (Bucurenciu et al., 2008; Bucurenciu et al., 2010; Eggermann and Jonas, 2012). The spatial grid resolution was 1 nm. Finally, the transmitter release rate was computed from the Ca^{2+} concentration, using a previously published model of the Ca^{2+} sensor of exocytosis (Sun et al., 2007), defining the Q matrix and the corresponding set of ordinary differential equations. Partial and ordinary differential equations were numerically solved using NDSolve of Mathematica 8.0 (Wolfram Research) running on a 12-core PC under Debian-Gnu Linux. As simulations were highly demanding regarding computation time and memory usage, we simulated Ca^{2+} channel opening, Ca^{2+} diffusion, and release during a 1500 ms pulse to −60 mV.

The structure and the parameters of the model were similar to those reported previously (Bucurenciu et al., 2008, 2010; Eggermann and Jonas, 2012). The bouton was modeled as a hemisphere with a radius (r_{max}) of 500 nm. A Ca^{2+} point source was implemented at the center of the planar surface, whereas a Ca^{2+} extrusion mechanism was placed on the hemispheric periphery. The affinities of mobile Ca^{2+} buffers (ATP) and endogenous fixed Ca^{2+} buffers were assumed as 200 and 2 μM, respectively, and the binding rates for Ca^{2+} were chosen as $5 \times 10^8\ M^{-1}\ s^{-1}$ in

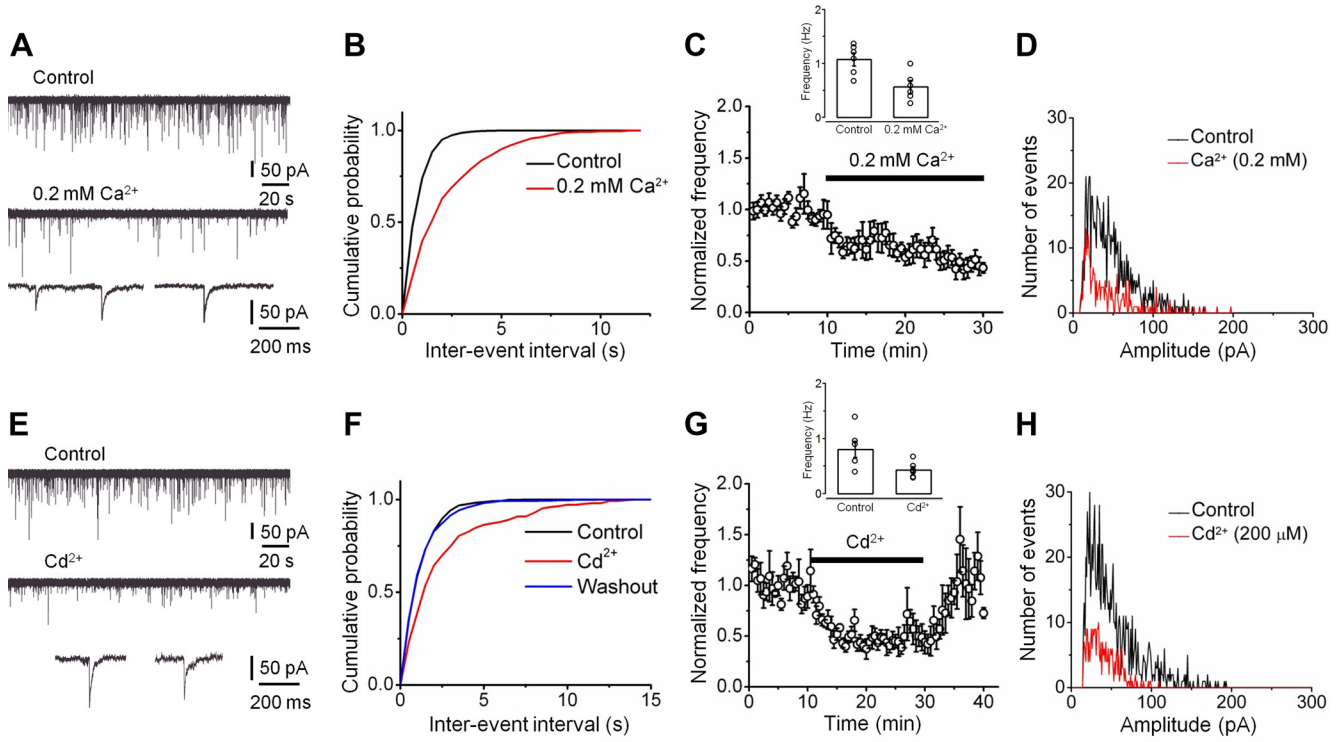

Figure 2. Miniature IPSC frequency depends on extracellular Ca^{2+} concentration and spontaneous opening of voltage-gated Ca^{2+} channels. ***A***, Original traces of mIPSCs at −80 mV. Top, Control conditions (2 mM extracellular Ca^{2+}); center, events in the presence of 0.2 mM extracellular Ca^{2+}; bottom, expanded traces for the two conditions. ***B***, Cumulative distribution of mIPSC inter-event intervals for a representative experiment in control (black) and 0.2 mM Ca^{2+} (red). Same experiment as shown in ***A***. ***C***, Plot of mean normalized frequency of mIPSCs against time. Average data from six experiments. Inset, Summary bar graph of mIPSC frequency for the two conditions. ***D***, Peak amplitude histograms in 0.2 mM extracellular Ca^{2+} and control conditions from a representative experiment. Histograms taken from epochs of identical duration (10 min). ***E–H,*** Original traces of mIPSCs (***E***), cumulative histogram of mIPSC inter-event interval for a representative experiment (***F***; black, control; red, 200 μM extracellular Cd^{2+}, blue, washout), plot of mean normalized frequency of mIPSCs against time (***G***), and peak amplitude histograms (***H***) illustrating the effects of 200 μM Cd^{2+} (6 cells). Mean amplitudes 46.7 pA (control) and 41.1 pA (0.2 Ca^{2+}) in ***D*** and 50.4 pA (control) and 43.1 pA (Cd^{2+}) in ***H*** for representative experiments shown. In all experiments, 1 μM TTX, 10 μM CNQX, and 20 μM D-AP5 were added to the bath solution to pharmacologically isolate mIPSCs.

both cases. The concentration of mobile Ca^{2+} buffers was assumed as 290 μM. The concentration of the fixed Ca^{2+} buffers was chosen as 160 μM, two-fold higher than at the calyx of Held (Meinrenken et al., 2002) to account for the higher endogenous Ca^{2+}-binding ratio of inhibitory interneurons (Aponte et al., 2008). The resting Ca^{2+} concentration was set to 71 nM, as previously measured in fast-spiking interneurons using 100 μM fura-2 (Aponte et al., 2008). The diffusion coefficients for Ca^{2+} ions (D_{Ca}) and mobile Ca^{2+} buffer (D_B) were assumed as $D_{Ca} = D_B = 220\ \mu m^2\ s^{-1}$. The Ca^{2+} extrusion mechanism was implemented with the boundary condition, as follows:

$$\frac{\partial[Ca^{2+}]}{\partial r} + \frac{M}{D_{Ca}} \frac{[Ca^{2+}]}{[Ca^{2+}] + K_p} = 0 \quad \text{for } r \rightarrow r_{max},$$

where M is the maximal pump rate and K_p is the dissociation constant (Matveev et al., 2004). M was assumed as 0.01 μM μm ms^{-1} and K_p was set to 0.2 μM (Matveev et al., 2004). The main free parameters in the model were Ca^{2+} extrusion rate, Ca^{2+} buffer concentration, and affinity of the Ca^{2+} sensor, which were varied over a 100-fold range.

Results

Miniature IPSC frequency in hippocampal granule cells is higher than miniature EPSC frequency

To elucidate the mechanisms of spontaneous transmitter release at different synapses, we recorded both mIPSCs and mEPSCs in dentate gyrus granule cells under standard conditions of pharmacological isolation (Fig. 1). mIPSCs were measured in the presence of 10 μM CNQX and 20 μM D-AP5, whereas mEPSCs were recorded in the presence of 10 μM bicuculline methiodide. In both cases, 1 μM TTX was added to the bath solution to suppress presynaptic action potential activity.

Several differences were detected between mIPSCs and mEPSCs in dentate gyrus granule cells. First, the amplitude was significantly larger for mIPSCs (median 37.1 ± 1.2 pA, 66 cells; Fig. 1*D*) than for mEPSCs (13.3 ± 0.39 pA, 37 cells; $p < 0.0001$; Fig. 1*G*). Second, the rise time was slightly slower for mIPSCs than for mEPSCs (median 1.16 ± 0.07 ms vs 0.90 ± 0.04 ms; $p < 0.0001$; Fig. 1*E*,*H*). Finally, despite the abundance of excitatory synapses on the dendritic tree of granule cells, the frequency of mIPSCs was substantially higher than that of mEPSCs recorded under identical conditions (mean 1.07 ± 0.07 Hz vs 0.29 ± 0.03 Hz; $p < 0.0001$; Fig. 1*F*,*I*). These results indicate that miniature postsynaptic currents in dentate gyrus granule cells are primarily generated at inhibitory synapses (Soltesz et al., 1995), whereas excitatory synapses play a secondary role.

Miniature IPSC frequency is dependent on both extracellular Ca^{2+} concentration and presynaptic Ca^{2+} channel opening

To test whether the high frequency of mIPSCs was Ca^{2+} dependent, we changed the extracellular Ca^{2+} concentration from 2 to 0.2 mM (Fig. 2). Reduction of the extracellular Ca^{2+} concentration significantly reduced the frequency of mIPSCs to 53.1 ± 8.4% of the control value ($p < 0.05$; Fig. 2*A–D*; Table 1). In contrast, the peak amplitude of mIPSCs was not significantly affected, changing to 93.1 ± 5.5% in the same set of experiments ($p > 0.1$; Table 1). These results confirm previous findings that spontaneous release at some synapses depends on the extracellu-

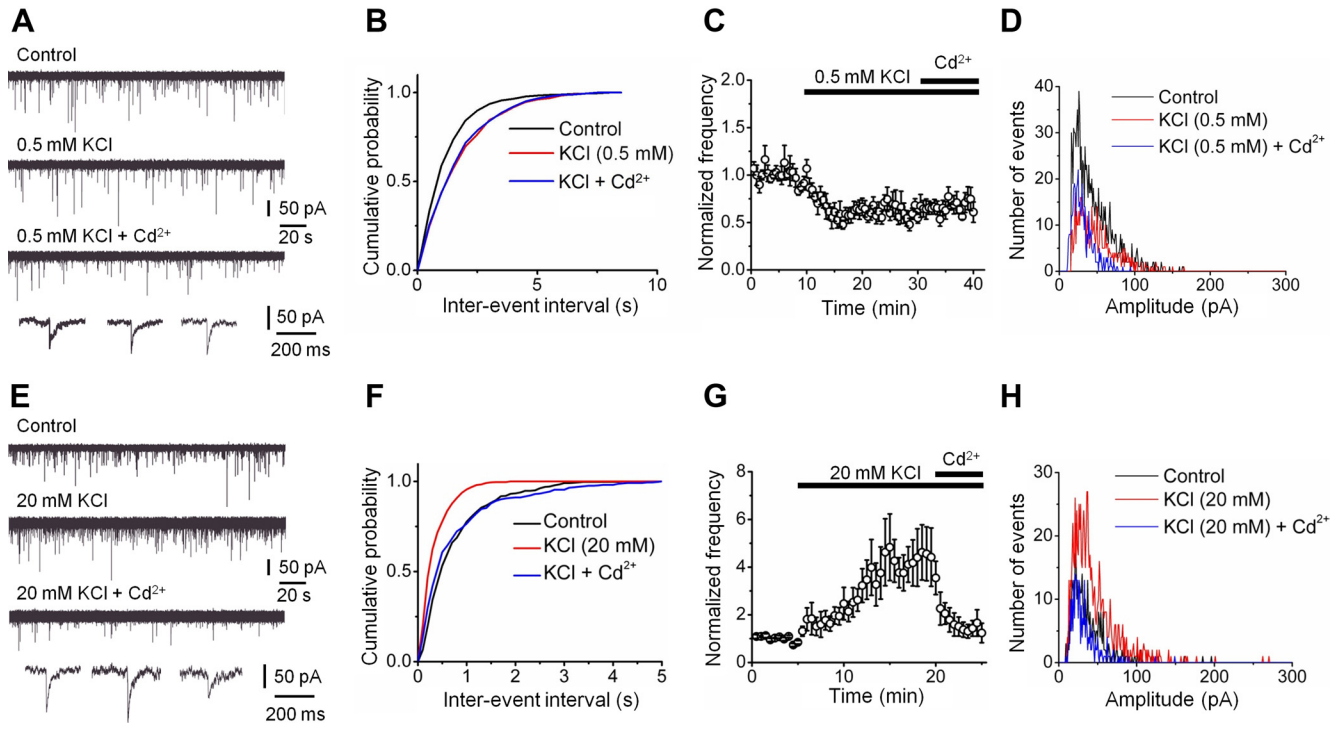

Figure 3. Miniature IPSC frequency depends on the presynaptic resting membrane potential. ***A***, Original traces of mIPSCs recorded at −80 mV. Top, Control conditions; upper center, events in the presence of 0.5 mM extracellular KCl; lower center, events in the presence of 0.5 mM KCl + 200 μM Cd^{2+}; bottom, expanded traces for the three conditions. ***B***, Cumulative distribution of mIPSC inter-event intervals for a representative experiment in control (black), 0.5 mM KCl (red), and 0.5 mM KCl + 200 μM Cd^{2+} (blue). Same experiment as shown in ***A***. ***C***, Plot of mean normalized frequency of mIPSCs against time. Average data from five experiments. ***D***, Peak amplitude histograms in control (black), 0.5 mM KCl (red), and 0.5 mM KCl + 200 μM Cd^{2+} (blue) from a representative experiment. ***E–H,*** Original traces (***E***), cumulative inter-event interval distributions (***F***), plot of mean normalized frequency against time (***G***), and peak amplitude histograms before and during application of 20 mM KCl and 20 mM KCl + 200 μM Cd^{2+} from a representative experiment (***H***). Data from six experiments. Mean amplitudes 44.6 pA (control), 51.2 pA (0.5 mM K^+), and 30.3 pA (0.5 mM K^+ + Cd^{2+}) in ***D*** and 37.5 pA (control), 43.7 pA (20 mM K^+), and 33.1 pA (20 mM K^+ + Cd^{2+}) in ***H*** for representative experiments shown. Histograms in ***D*** and ***H*** taken from epochs of identical duration (10 and 5 min, respectively).

lar Ca^{2+} concentration (Llano et al., 2000; Angleson and Betz, 2001; Vyleta and Smith, 2011).

To identify the Ca^{2+} sources that mediate the dependence of mIPSC frequency on extracellular Ca^{2+} concentration, we first tested the effects of the unselective Ca^{2+} channel blocker Cd^{2+}, which inhibits multiple types of Ca^{2+} channels (Fig. 2*E–H*). When applied at a saturating concentration (200 μM) (Randall, 1998), Cd^{2+} significantly, rapidly, and reversibly reduced the frequency of mIPSCs to 53.5 ± 5.3% of control at ~22°C ($p < 0.05$; Fig. 2*E–H*; Table 1). Almost identical effects were obtained at ~32°C (55.1 ± 10.1% of control; Table 1). The effect of 200 μM Cd^{2+} was similar to that of 0.2 mM Ca^{2+} ($p > 0.1$). In contrast, Cd^{2+} had no significant effect on mIPSC amplitude (Table 1). Our results indicate that spontaneous release at inhibitory synapses on granule cells is comprised of a Ca^{2+}-independent and a Ca^{2+}-dependent component. Furthermore, our data suggest that the Ca^{2+}-dependent component is mediated by spontaneous opening of voltage-gated Ca^{2+} channels.

If voltage-gated Ca^{2+} channels represent the primary source of Ca^{2+} inflow driving spontaneous release, changes in the presynaptic resting potential would alter the probability of presynaptic Ca^{2+} channel opening and thereby affect their contribution to spontaneous transmitter release (Awatramani et al., 2005). To test this prediction, we changed the presynaptic membrane potential by manipulation of the extracellular K^+ concentration (Fig. 3). Reduction of extracellular K^+ concentration from 2 to 0.5 mM reduced the frequency of mIPSCs to 56.7 ± 5.9% of the control value. Subsequent application of Cd^{2+} under these experimental conditions had no significant effect on mIPSC frequency ($p > 0.1$; Fig. 3*A–D*; Table 1). Conversely, increasing the extracellular K^+ concentration from 2 to 20 mM increased the frequency of mIPSCs to 360.7 ± 70.1% of control. Furthermore, subsequent application of Cd^{2+} had markedly enhanced inhibitory effects (42.9 ± 5.0% reduction in 200 μM Cd^{2+} + 20 mM K^+ versus 20 mM K^+; $p < 0.05$; Fig. 3*E–H*; Table 1). These results are consistent with the hypothesis that stochastic opening of voltage-gated Ca^{2+} channels in inhibitory presynaptic terminals triggers spontaneous transmitter release.

Miniature release is driven by opening of N- and L-type Ca^{2+} channels

To further determine the types of Ca^{2+} channel involved in spontaneous release at inhibitory synapses, we systematically tested the effects of several specific Ca^{2+} channel blockers (Randall and Tsien, 1995) (Fig. 4). The P/Q-type Ca^{2+} channel blocker ω-agatoxin IVa (1 μM) had no significant effects on the frequency of mIPSCs (101 ± 9% of control value; Fig. 4*A–C*). In contrast, the N-type Ca^{2+} channel blocker ω-conotoxin GVIa (1 μM) markedly reduced the mIPSC frequency (to 77.0 ± 5.9% of control value, $p < 0.05$; Fig. 4*D–F*; Table 1). Similarly, the L-type Ca^{2+} channel blocker nimodipine (20 μM) reduced the mIPSC frequency (to 79.1 ± 4% of control; $p < 0.05$; Fig. 4*G–I*; Table 1). To corroborate the validity of our pharmacological dissection, we tested the effects of the L-type Ca^{2+} channel activator Bay K 8644. Bay K 8644 (20 μM) increased the frequency of mIPSC to 128.5 ± 10.2% of the preceding control value ($p < 0.05$; Table 1). Finally, neither the T-type Ca^{2+} channel blocker NNC 55-0396 (10 μM, a mibefradil analog with increased selectivity for T-type channels)

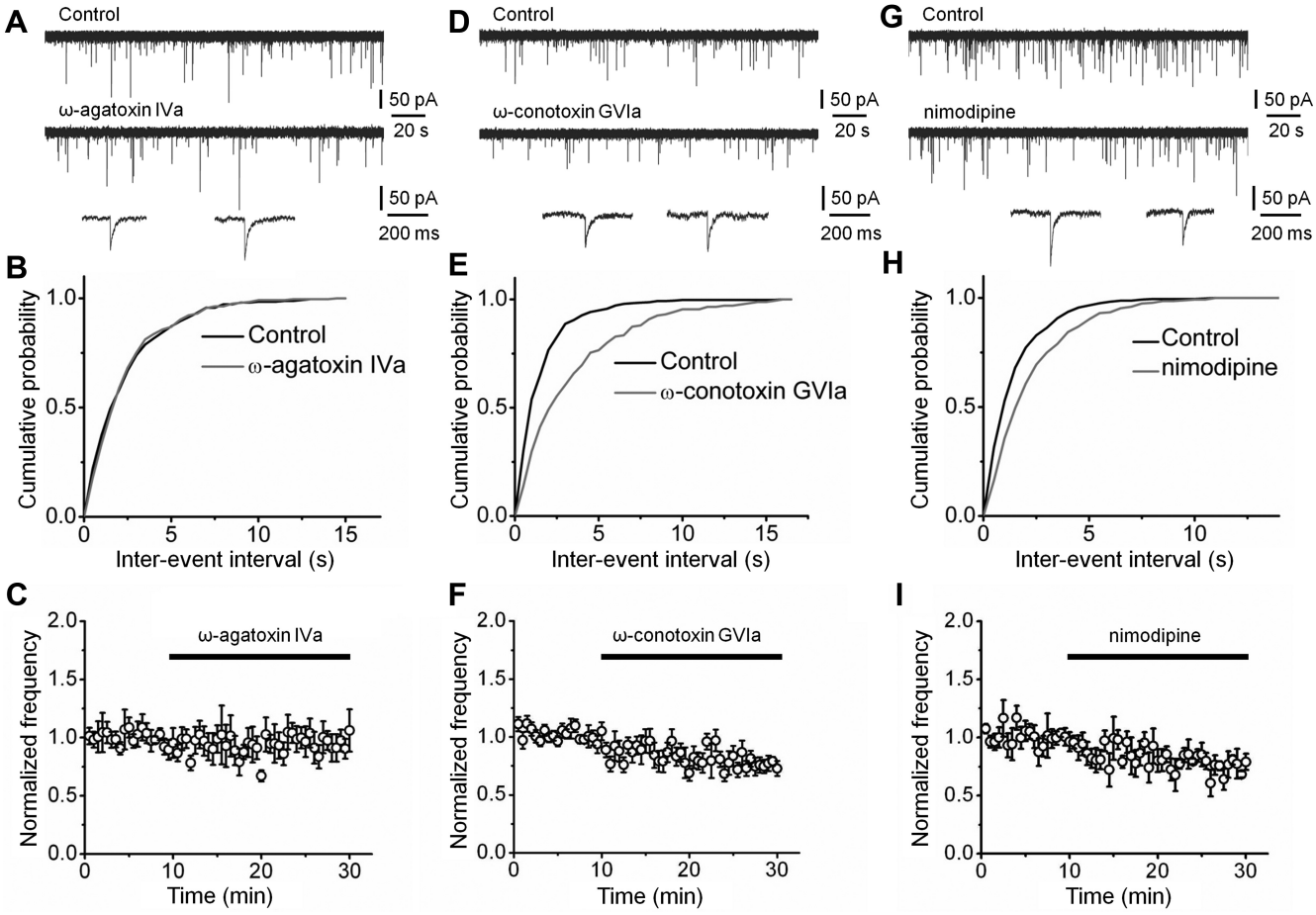

Figure 4. Openings of presynaptic N- and L-type Ca^{2+} channels make a substantial contribution to spontaneous release. ***A***, Original traces of mIPSCs recorded at −80 mV. Top, Control conditions; center, events in the presence of 1 μM extracellular ω-agatoxin IVa; bottom, expanded traces for the two conditions. ***B***, Cumulative distribution of mIPSC inter-event intervals for a representative experiment in control (black) and ω-agatoxin IVa (gray). Same experiment as shown in ***A***. ***C***, Plot of mean normalized frequency of mIPSCs against time. Average data from seven experiments. ***D–F,*** Original traces (***D***), cumulative inter-event interval distributions (***E***), and plot of mean normalized frequency against time (***F***) before and during application of 1 μM ω-conotoxin GVIa (10 cells). ***G–I***, Original traces (***G***), cumulative inter-event interval distributions (***H***), and plot of mean normalized frequency against time (***I***) before and during application of 20 μM nimodipine (5 cells).

(Huang et al., 2004) nor the R-type Ca^{2+} channel blocker SNX-482 (500 nM) (Newcomb et al., 1998; Li et al., 2007) had any effect on mIPSC frequency (Table 1). In addition, none of the specific Ca^{2+} channel blockers tested had any effect on mIPSC amplitude (Table 1). In conclusion, these results suggest that N-type and L-type Ca^{2+} channels are the primary sources of Ca^{2+} inflow that drives spontaneous release at inhibitory synapses on granule cells.

In the dentate gyrus, evoked release from the synapses of PV-expressing basket cells exclusively relies on P/Q-type Ca^{2+} channels, whereas that from synapses of cholecystokinin (CCK)-expressing interneurons selectively involves N-type Ca^{2+} channels (Poncer et al., 1997; Hefft and Jonas, 2005). To determine whether N-type Ca^{2+} channels relevant for the regulation of spontaneous release were located on synapses of CCK interneurons, we made use of the selective presence of CB_1 endocannabinoid receptors on CCK terminals (Katona et al., 1999; Wilson et al., 2001; Yamasaki et al., 2006) (Fig. 5). Bath application of the CB_1 receptor agonist WIN 55212-2 (3 μM) markedly reduced the frequency of mIPSCs (74.9 ± 4.3% of control value, $p < 0.05$; Fig. 5*A–C*; Table 1). The effect of WIN 55212-2 on mIPSC frequency was similar to that of ω-conotoxin GVIa ($p > 0.1$). Furthermore, the inhibitory effect of WIN 55212-2 was occluded by prior application of ω-conotoxin GVIa; on average, the mIPSC frequency in the presence of WIN 55212-2 + ω-conotoxin GVIa was 101.9 ± 10.2% of the corresponding value in ω-conotoxin GVIa ($p > 0.1$; Fig. 5*D–F*; Table 1). Taken together, these results suggest that the N-type Ca^{2+} channels responsible for spontaneous release were primarily located on the synaptic terminals of CCK interneurons. To address whether N- and L-type channels were present on the same presynaptic terminals, we tested combined application of N- and L-type channel blockers. On average, the mIPSC frequency in the presence of ω-conotoxin GVIa + nimodipine was 101.9 ± 5.8% of the corresponding value in nimodipine ($p > 0.1$; Table 1). Thus, occlusion of blocker effects suggests that N- and L-type Ca^{2+} channels are located on the same presynaptic terminals, and that these terminals are identical to the ones that express CB_1 receptors and release the peptide CCK (Freund, 2003).

Spontaneous release is driven by spatially extended Ca^{2+} domains

To examine whether Ca^{2+} nanodomains or microdomains were involved in spontaneous release events, we tested the effects of the fast Ca^{2+} chelator BAPTA and the slow Ca^{2+} chelator EGTA on spontaneous release (Adler et al., 1991) (Fig. 6). Both chelators were applied in membrane-permeant ester forms. Application of 100 μM BAPTA-AM significantly reduced the frequency of mIP-

SCs to 56.8 ± 3.4% of the control value ($p < 0.05$; Fig. 6*A–C*; Table 1). Likewise, application of 100 μM EGTA-AM reduced the frequency of mIPSCs to 60.9 ± 6.5% of control ($p < 0.05$; Fig. 6*D–F*; Table 1). The reduction in mIPSC frequency by EGTA-AM was similar to that with BAPTA-AM ($p > 0.1$), suggesting that the effects of the Ca^{2+} chelators correlated more closely with the affinity values than with Ca^{2+}-binding rates (Neher, 1998). Thus, spontaneous release at inhibitory synapses is driven by a microdomain rather than nanodomain coupling configuration between Ca^{2+} channels and Ca^{2+} sensors.

Our finding that Ca^{2+} chelators suppress spontaneous release appears inconsistent with a simple model, in which the basal Ca^{2+} concentration under steady-state conditions drives release (Neher, 1998). Thus, we explored more realistic scenarios where release was triggered by Ca^{2+} domains generated by phasic Ca^{2+} channel opening (Fig. 7). The finding that CCK terminals using microdomain coupling for evoked release contribute more to spontaneous release than PV terminals using nanodomain coupling for evoked release may be surprising, since stochastic effects are expected to be larger in the nanodomain coupling regime (Meinrenken et al., 2002). To resolve this possible paradox, we simulated spontaneous transmitter release using stochastic models of both microdomain and nanodomain coupling regimes (Bucurenciu et al., 2010) (Fig. 7). To account for the high probability of evoked release at CCK terminals (Daw et al., 2009), the reduction of Ca^{2+} transients with increasing coupling distance was compensated by a proportional increase in the number of channels. Analysis of relation between mean release rate and coupling distance showed a minimum at ~40 nm, corresponding to ~6 Ca^{2+} channels in our model, but elevated release at both smaller and larger distances (Fig. 7*G*). Thus, both nanodomain and microdomain coupling regimes can generate high rates of spontaneous release. However, the mechanisms were different in the two scenarios. In the case of microdomain coupling, stochastic Ca^{2+} channel openings generated a slow elevation of the Ca^{2+} concentration (Fig. 7*B*,*C*). Although the spontaneous opening of single channel was not sufficient for transmitter release in this coupling configuration, superposition of Ca^{2+} transients from multiple channels efficiently drove transmitter release. In contrast, in the case of nanodomain coupling, stochastic Ca^{2+} channel openings generated brief Ca^{2+} transients, which translated into temporally associated release events (Fig. 7*E*,*F*).

To identify the conditions under which synapses with loose coupling would produce higher spontaneous release rates than those with tight coupling, we examined the dependence of mean release rate on the Ca^{2+} extrusion rate (representing, e.g., Na^+/Ca^{2+} exchangers and Ca^{2+}-ATPases; Fig. 7*H*), the total endogenous buffer concentration (varied by changing the concentrations of fixed and mobile buffers by the same factor; Fig. 7*I*), the affinity of the Ca^{2+} sensor of exocytosis (varied by changing the Ca^{2+} unbinding rate k_{off} and δ; Fig. 7*J*) (Sun et al., 2007), and the voltage range of Ca^{2+} channel activation (Fig. 7*K*). In our model, the mean release rate at synapses with loose coupling exceeded the average release rate at synapses with tight coupling under several conditions: (1) low Ca^{2+} extrusion rate, (2) low total Ca^{2+} buffer concentration, (3) high Ca^{2+} sensor affinity, and (4) left-shifted Ca^{2+} channel activation curves.

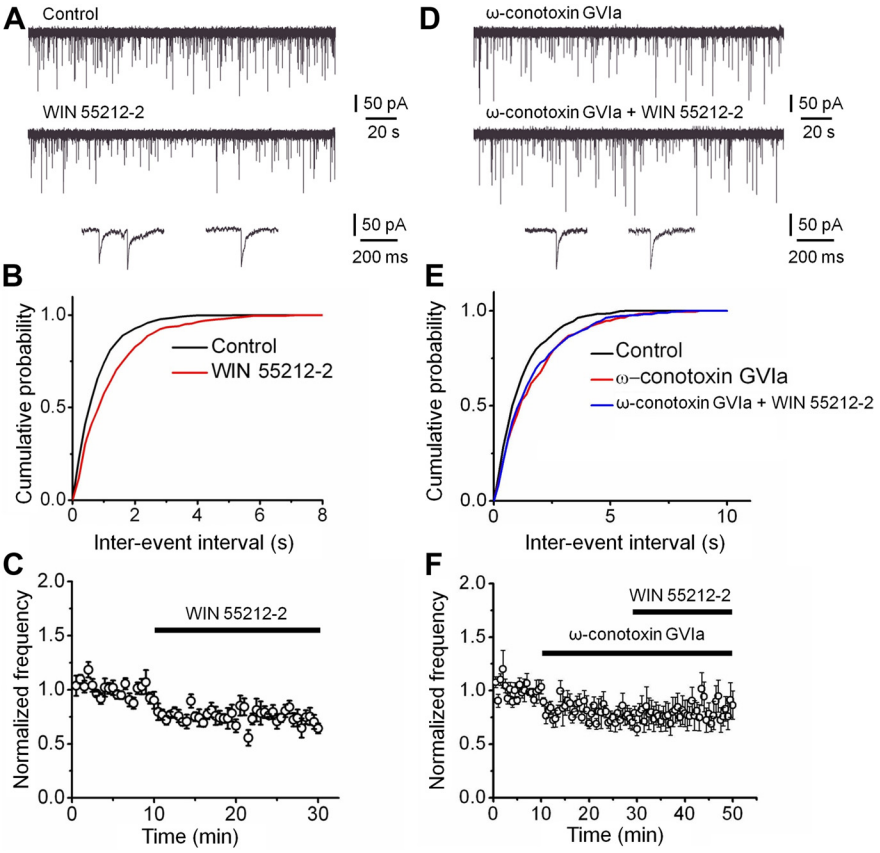

Figure 5. CCK terminals make a substantial contribution to Ca^{2+}-dependent miniature release. ***A***, Original traces of mIPSCs recorded at −80 mV. Top, Control conditions; center, events in the presence of 3 μM WIN 55212-2; bottom, expanded traces for the two conditions. ***B***, Cumulative distribution of mIPSC inter-event intervals for a representative experiment in control (black) and WIN 55212-2 (red). Same experiment as shown in ***A***. ***C***, Plot of mean normalized frequency of mIPSCs against time. Average data from six experiments. ***D–F,*** Original traces (***D***), cumulative inter-event interval distributions (***E***), and plot of mean normalized frequency against time (***F***) in 1 μM ω-conotoxin GVIa and 1 μM ω-conotoxin GVIa + 3 μM WIN 55212-2 (6 cells). Note that the effects of WIN 55212-2 are occluded by prior application of ω-conotoxin GVIa.

Discussion

The present results revealed several unexpected properties of mIPSCs in hippocampal granule cells. First, while ~50% of mIPSCs were Ca^{2+} independent, ~50% were dependent on spontaneous opening of presynaptic Ca^{2+} channels. Second, Ca^{2+}-dependent release was dependent on the opening of N-type and L-type channels, but not P/Q-type Ca^{2+} channels. Third, Ca^{2+}-dependent spontaneous release was inhibited by both BAPTA-AM and EGTA-AM with comparable efficacy, suggesting that it was dependent on microdomain coupling between Ca^{2+} source and sensor. Finally, the sensitivity of mIPSC frequency to the CB_1 receptor agonist WIN 55212-2 suggests that a major portion of Ca^{2+}-dependent spontaneous release events is generated at the synaptic terminals of CCK interneurons. The preferential contribution of CCK interneurons to miniature events is highly unexpected, since CCK interneurons are present

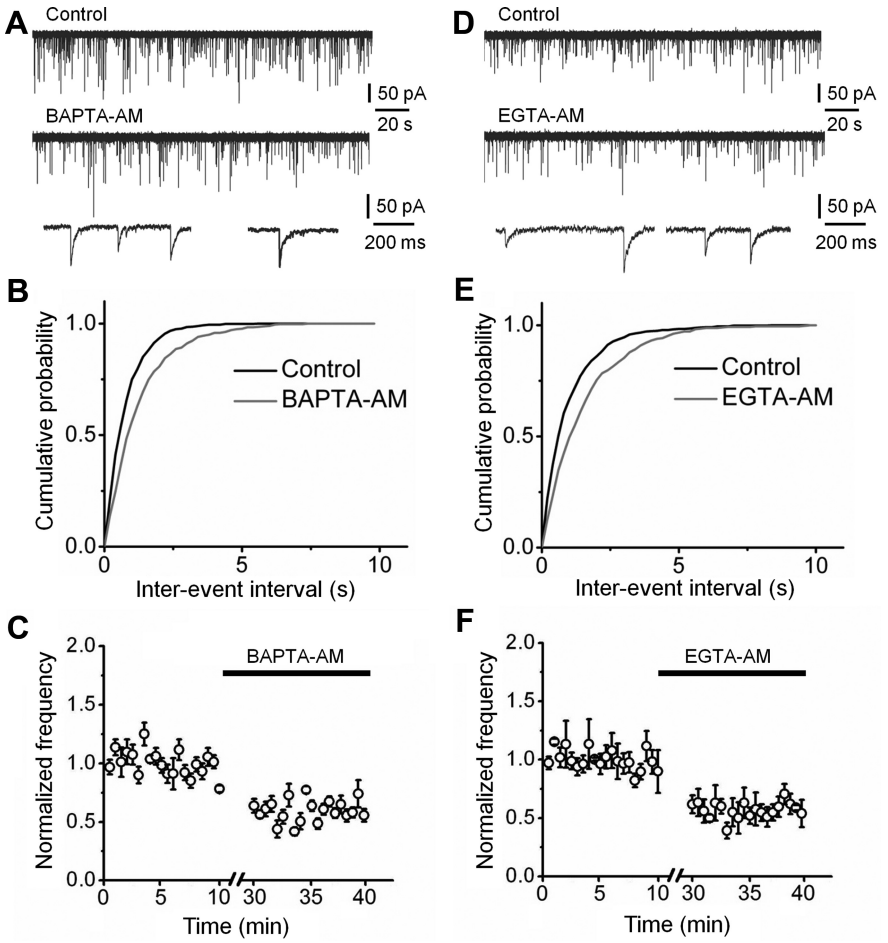

Figure 6. Ca^{2+}-dependent miniature release is driven by a microdomain coupling mechanism. ***A***, Original traces of mIPSCs at −80 mV. Top, Control conditions; center, events in the presence of 100 μM BAPTA-AM; bottom, expanded traces for the two conditions. ***B***, Cumulative distribution of mIPSC inter-event intervals for a representative experiment in control (black) and BAPTA-AM (gray). Same experiment as shown in ***A***. ***C***, Plot of mean normalized frequency of mIPSCs against time. Average data from five experiments. ***D–F,*** Original traces (***D***), cumulative inter-event interval distributions (***E***), and plot of mean normalized frequency against time (***F***) before and during application of 100 μM EGTA-AM (5 cells). Note that BAPTA-AM and EGTA-AM reduced the frequency of mIPSCs by approximately the same extent.

in small numbers and have relatively sparse axonal arborizations (Freund and Buzsáki, 1996; Hefft and Jonas, 2005).

Comparison between evoked and spontaneous release

At least six specific classes of GABAergic interneurons form inhibitory synapses on dentate gyrus granule cells. Axo-axonic cells, PV-expressing basket cells, and CCK-positive basket cells project to the axon initial segment, somata, and proximal dendrites of granule cells, respectively (Han et al., 1993; Freund and Buzsáki, 1996; McBain and Fisahn, 2001). In contrast, hilar commissural-associational pathway (HICAP) cells form a dense axonal plexus in the inner third of the molecular layer, while somatostatin-positive hilar perforant path (HIPP) cells and molecular layer interneurons innervate the distal apical dendrites of dentate gyrus granule cells (Han et al., 1993; Freund and Buzsáki, 1996; McBain and Fisahn, 2001) (Fig. 1*A*).

Previous studies revealed that the properties of evoked release substantially differ between these different types of GABAergic synapses (Freund, 2003; Hefft and Jonas, 2005; Glickfeld and Scanziani, 2006). In PV interneuron output synapses, evoked release is driven by a small number of P/Q-type Ca^{2+} channels tightly coupled to Ca^{2+} sensors, resulting in highly synchronized release (Hefft and Jonas, 2005; Bucurenciu et al., 2008, 2010). By contrast, in CCK interneurons a presumably larger number of N-type channels is loosely coupled to the sensors, promoting asynchronous forms of transmitter release (Hefft and Jonas, 2005; Daw et al., 2009; Ali and Todorova, 2010). Furthermore, GABA release from CCK interneuron output synapses is specifically inhibited by CB_1 receptors (Katona et al., 1999; Wilson et al., 2001; Ali and Todorova, 2010).

As many different inputs converge on a given postsynaptic neuron, the precise synaptic origin of mIPSCs is often unknown. However, our results provide clues about which subsets of inhibitory synapses underlie spontaneous release. Our finding that both ω-conotoxin GVIa and CB_1 receptor antagonists suppress spontaneous release to the same extent and that their effects occlude each other indicates that a significant proportion of Ca^{2+}-dependent spontaneous release is generated at the output synapses of CCK interneurons (Katona et al., 1999; Pitler and Alger, 1994; Wilson et al., 2001; Yamasaki et al., 2006). Conversely, our result that ω-agatoxin IVa has no detectable effects on mIPSC frequency suggests that Ca^{2+}-dependent spontaneous release is not mediated by the output synapses of PV interneurons. Thus, the properties of spontaneous release are consistent with the marked differences between the properties of evoked release from CCK and PV interneurons (Hefft and Jonas, 2005).

The contribution of L-type Ca^{2+} channels to spontaneous inhibitory transmitter release was unexpected, since L-type Ca^{2+} channels do not contribute to GABA release evoked by single action potentials (Jensen and Mody, 2001) and L-type Ca^{2+} channel immunoreactivity is primarily found in dendrites (Westenbroek et al., 1990). However, these Ca^{2+} channels have been reported to contribute to post-tetanic potentiation at GABAergic synapses in the dentate gyrus (Jensen and Mody, 2001). Thus, L-type Ca^{2+} channels are likely to be also present in GABAergic presynaptic terminals.

Mechanisms of microdomain-driven spontaneous release

Our results reveal that a significant fraction of spontaneous release at inhibitory synapses on dentate gyrus granule cells is triggered by N- and L-type Ca^{2+} channels via Ca^{2+} microdomain coupling. How is it possible that spontaneous release is more effectively driven by Ca^{2+} microdomains than nanodomains? Modeling of stochastic Ca^{2+} channel opening and subsequent transmitter release suggests several possibilities (Fig. 7). First, the relation between mean release rate and coupling distance showed a minimum at ~40 nm, corresponding to ~6 Ca^{2+} channels, but elevated release at both smaller and larger distances (Fig. 7*G*). This implies that both extreme cases (20 and 200 nm coupling distance in our model) drive spontaneous release. A major assumption in our model is that channel number and coupling

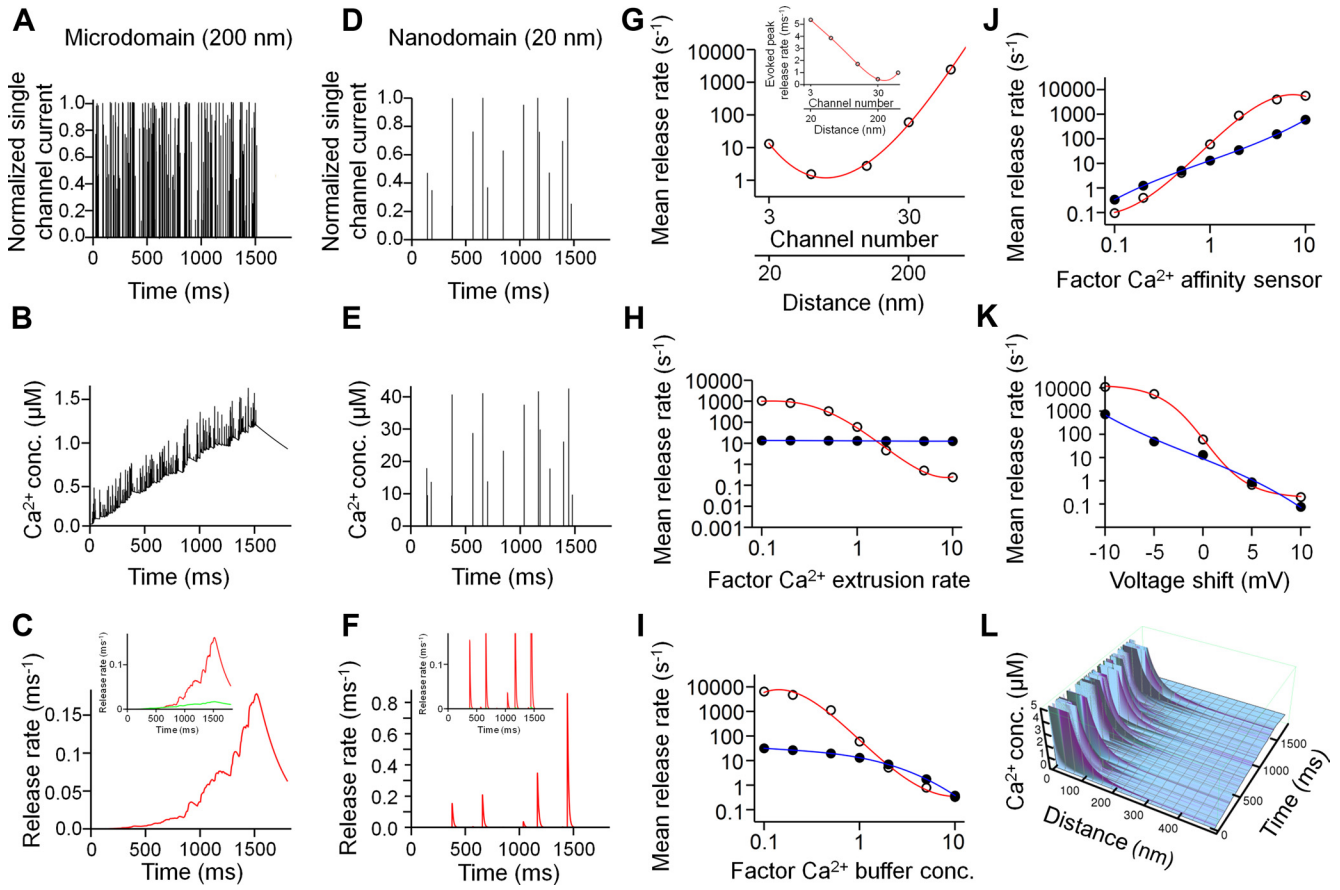

Figure 7. Stochastic model for miniature IPSC generation in nanodomain and microdomain coupling regimes. ***A–C***, Spontaneous Ca^{2+} channel opening (***A***), resulting intracellular Ca^{2+} transients at the sensor (***B***), and transmitter release rate (***C***) in a loose coupling configuration (200 nm coupling distance). A 1.5 s pulse from −80 mV to −60 mV was applied to increase release rate; 1.8 s total simulation time. ***D–F***, Spontaneous Ca^{2+} channel opening (***D***), resulting intracellular Ca^{2+} transients at the sensor (***E***), and transmitter release rate (***F***) in a tight coupling configuration (20 nm coupling distance). Insets in ***C*** and ***F*** indicate separately the components of synchronous (red) and asynchronous release (green), driven by different states in the Ca^{2+} sensor model (Sun et al., 2007). ***G***, Double logarithmic plot of mean spontaneous release rate against number of Ca^{2+} channels and distance between Ca^{2+} channels and sensor. Distance and channel number were increased in parallel to approximately maintain the probability of evoked release. Inset, Peak evoked release rate under similar conditions. ***H–K,*** Plot of mean spontaneous release rate against Ca^{2+} extrusion rate (***H***), Ca^{2+} buffer concentration (***I***), Ca^{2+} affinity of the sensor (***J***), and shift in the voltage dependence of Ca^{2+} channel activation (***K***) in loose (open circles, red curve) and tight (filled circles, blue curve) coupling configuration. In ***H–J***, the independent variable is given in normalized form, with a value of 1 corresponding to the default values of the model. In ***K***, the shift is given in absolute units (see Materials and Methods). Curves in ***G–K*** represent polynomial functions fit to the data points. Mean release rate was determined by dividing the maximum value of cumulative release by the total duration of the pulse to −60 mV. ***L***, Spatiotemporal extent of Ca^{2+} domains in the microdomain coupling configuration. Ca^{2+} concentration is plotted three-dimensionally against distance from the source and time (time axis similar as in ***B***). The Ca^{2+} source is comprised of 30 channels. Each peak in the plot near the source represents the opening of a single Ca^{2+} channel (maximal values near the source truncated). Note that release will be driven by a combination of microdomain Ca^{2+} and basal Ca^{2+} "seen" by the Ca^{2+} sensor.

distance change in parallel, maintaining the probability of evoked release. This assumption seems justified, based on the experimental observation that PV and CCK terminals differ in coupling distance, but show comparable probability of evoked release (Kraushaar and Jonas, 2000; Hefft and Jonas, 2005; Daw et al., 2009).

Second, our model suggests that synapses with loose coupling of a large number of channels (CCK-like) generate spontaneous release at higher frequency than synapses with tight coupling of a small number of channels (PV-like) in a substantial portion of the simulated parameter space. In particular, a high frequency of spontaneous release is observed under conditions of low Ca^{2+} extrusion rate, low endogenous Ca^{2+} buffer concentration, high affinity of the Ca^{2+} sensor of transmitter release, and left-shifted Ca^{2+} channel activation curves. Is there any direct experimental evidence for such differences between PV- and CCK-expressing interneurons? For the Ca^{2+} extrusion rate, it is possible that the major transporters, Na^{+}/Ca^{2+} exchangers or Ca^{2+}-ATPases (Kim et al., 2005), are differentially expressed. For the endogenous buffer capacity, both the high endogenous Ca^{2+}-binding ratio in PV cells (κ_s ~200) (Aponte et al., 2008) and the large extent and long duration of asynchronous release in CCK interneurons suggest a substantial difference (high buffer concentration in PV cells versus low buffer concentration in CCK cells). Regarding the affinity of the Ca^{2+} sensor, it is possible that the putative Ca^{2+} sensors synaptotagmin (Geppert et al., 1994; Sun et al., 2007; Kerr et al., 2008; Xu et al., 2009) or Doc2 (Groffen et al., 2010; Yao et al., 2011; but see Pang et al., 2011) are differentially expressed between PV- and CCK-interneurons. Regarding Ca^{2+} channel gating, subtle differences in the activation curves of P/Q-, N-, and L-type Ca^{2+} channels in different presynaptic terminals could have large impact. Although the gating properties of P/Q- and N-type channels have been reported to be very similar (Li et al., 2007), additional functional differences may be conveyed by β-subunits, syntaxin binding, G-protein modulation, or channel phosphorylation (for review, see Catterall, 2011). Finally, differences in presynaptic resting potential may contribute. If HCN channels were expressed more densely in CCK than in PV interneurons, presynaptic terminals would be more depolarized,

and spontaneous opening of presynaptic Ca^{2+} channels will occur more frequently (Aponte et al., 2006).

Compared with the Ca^{2+}-dependent spontaneous release studied extensively in this paper, the Ca^{2+}-independent spontaneous release component remains mechanistically less clear. One possibility is that this second component is in fact Ca^{2+} dependent, but the affinity of the corresponding sensor is so high that the sensor is fully saturated under resting conditions. Alternatively, the Ca^{2+}-independent spontaneous release component may reflect "spontaneous fusion willingness," as represented by a transition from the unbound state of the Ca^{2+} sensor in kinetic schemes (Lou et al., 2005; Sun et al., 2007). It is possible that these mechanisms differentially operate in different types of inhibitory synapses. For example, it is conceivable that GABAergic terminals of PV interneurons make a large contribution to Ca^{2+}-independent spontaneous release.

Functional significance

Spontaneous generation of mIPSCs will have substantial effects on excitability of postsynaptic target cells. This is particularly the case in small neurons, like hippocampal and cerebellar granule cells (Carter and Regehr, 2002). The high frequency of spontaneous IPSCs in granule cells implements a form of tonic inhibition (Farrant and Nusser, 2005). As this inhibition is fluctuating, it would be expected to change the gain rather than the offset of neuronal input–output relations (Mitchell and Silver, 2003). A potential advantage of spontaneous release mediated by opening of N-type Ca^{2+} channels is that this form of inhibition can be regulated by CB_1 receptors (Pitler and Alger, 1994; Yamasaki et al., 2006). Thus, spontaneous release represents a tonic, fluctuating, and modifiable form of inhibition of dentate gyrus granule cells.

Spontaneous release of GABA may play an important role for signal processing in the hippocampal network. The high ratio of mIPSCs to mEPSCs in granule cells at rest may explain why these neurons generate action potentials sparsely under *in vivo* conditions. Thus, the high mIPSC to mEPSC frequency ratio may contribute to both sparse coding (Jung and McNaughton, 1993) and pattern separation in the dentate gyrus (Leutgeb et al., 2007).

Finally, the high spontaneous release rate may have long-term effects on synaptic structure. At excitatory hippocampal synapses, mEPSCs play an important role in the regulation of local postsynaptic protein synthesis (Sutton et al., 2006), the stabilization of excitatory synaptic function, and the maintenance of dendritic spines (McKinney et al., 1999). Whether mIPSCs also have long-term trophic functions, for example on newly generated granule cells (Overstreet Wadiche et al., 2005), remains to be determined.

References

Adler EM, Augustine GJ, Duffy SN, Charlton MP (1991) Alien intracellular calcium chelators attenuate neurotransmitter release at the squid giant synapse. J Neurosci 11:1496–1507.

Ahmed MS, Siegelbaum SA (2009) Recruitment of N-Type Ca^{2+} channels during LTP enhances low release efficacy of hippocampal CA1 perforant path synapses. Neuron 63:372–385.

Ali AB, Todorova M (2010) Asynchronous release of GABA via tonic cannabinoid receptor activation at identified interneuron synapses in rat CA1. Eur J Neurosci 31:1196–1207.

Angleson JK, Betz WJ (2001) Intraterminal Ca^{2+} and spontaneous transmitter release at the frog neuromuscular junction. J Neurophysiol 85:287–294.

Aponte Y, Lien CC, Reisinger E, Jonas P (2006) Hyperpolarization-activated cation channels in fast-spiking interneurons of rat hippocampus. J Physiol 574:229–243.

Aponte Y, Bischofberger J, Jonas P (2008) Efficient Ca^{2+} buffering in fast-spiking basket cells of rat hippocampus. J Physiol 586:2061–2075.

Awatramani GB, Price GD, Trussell LO (2005) Modulation of transmitter release by presynaptic resting potential and background calcium levels. Neuron 48:109–121.

Borst JGG, Sakmann B (1998) Calcium current during a single action potential in a large presynaptic terminal of the rat brainstem. J Physiol 506:143–157.

Bucurenciu I, Kulik A, Schwaller B, Frotscher M, Jonas P (2008) Nanodomain coupling between Ca^{2+} channels and Ca^{2+} sensors promotes fast and efficient transmitter release at a cortical GABAergic synapse. Neuron 57:536–545.

Bucurenciu I, Bischofberger J, Jonas P (2010) A small number of open Ca^{2+} channels trigger transmitter release at a central GABAergic synapse. Nat Neurosci 13:19–21.

Carter AG, Regehr WG (2002) Quantal events shape cerebellar interneuron firing. Nat Neurosci 5:1309–1318.

Catterall WA (2011) Voltage-gated calcium channels. Cold Spring Harb Perspect Biol 3:a003947.

Christie JM, Chiu DN, Jahr CE (2011) Ca^{2+}-dependent enhancement of release by subthreshold somatic depolarization. Nat Neurosci 14:62–68.

Clements JD, Bekkers JM (1997) Detection of spontaneous synaptic events with an optimally scaled template. Biophys J 73:220–229.

Daw MI, Tricoire L, Erdelyi F, Szabo G, McBain CJ (2009) Asynchronous transmitter release from cholecystokinin-containing inhibitory interneurons is widespread and target-cell independent. J Neurosci 29:11112–11122.

Denker A, Kröhnert K, Bückers J, Neher E, Rizzoli SO (2011) The reserve pool of synaptic vesicles acts as a buffer for proteins involved in synaptic vesicle recycling. Proc Natl Acad Sci U S A 108:17183–17188.

Eggermann E, Jonas P (2012) How the "slow" Ca^{2+} buffer parvalbumin affects transmitter release in nanodomain coupling regimes at GABAergic synapses. Nat Neurosci 15:20–22.

Eggermann E, Bucurenciu I, Goswami SP, Jonas P (2012) Nanodomain coupling between Ca^{2+} channels and sensors of exocytosis at fast mammalian synapses. Nat Rev Neurosci 13:7–21.

Farrant M, Nusser Z (2005) Variations on an inhibitory theme: phasic and tonic activation of $GABA_A$ receptors. Nat Rev Neurosci 6:215–229.

Freund TF (2003) Interneuron diversity series: rhythm and mood in perisomatic inhibition. Trends Neurosci 26:489–495.

Freund TF, Buzsáki G (1996) Interneurons of the hippocampus. Hippocampus 6:347–470.

Geppert M, Goda Y, Hammer RE, Li C, Rosahl TW, Stevens CF, Südhof TC (1994) Synaptotagmin I: a major Ca^{2+} sensor for transmitter release at a central synapse. Cell 79:717–727.

Glickfeld LL, Scanziani M (2006) Distinct timing in the activity of cannabinoid-sensitive and cannabinoid-insensitive basket cells. Nat Neurosci 9:807–815.

Goswami SP, Jonas P, Bucurenciu I (2011) Differential dependence of miniature IPSC and EPSC frequency on presynaptic Ca^{2+} channels at hippocampal synapses. Soc Neurosci Abstr 37:446.07.

Groffen AJ, Martens S, Díez Arazola R, Cornelisse LN, Lozovaya N, de Jong AP, Goriounova NA, Habets RL, Takai Y, Borst JG, Brose N, McMahon HT, Verhage M (2010) Doc2b is a high-affinity Ca^{2+} sensor for spontaneous neurotransmitter release. Science 327:1614–1618.

Han ZS, Buhl EH, Lörinczi Z, Somogyi P (1993) A high degree of spatial selectivity in the axonal and dendritic domains of physiologically identified local-circuit neurons in the dentate gyrus of the rat hippocampus. Eur J Neurosci 5:395–410.

He L, Xue L, Xu J, McNeil BD, Bai L, Melicoff E, Adachi R, Wu LG (2009) Compound vesicle fusion increases quantal size and potentiates synaptic transmission. Nature 459:93–97.

Hefft S, Jonas P (2005) Asynchronous GABA release generates long-lasting inhibition at a hippocampal interneuron–principal neuron synapse. Nat Neurosci 8:1319–1328.

Hoffman AF, Lupica CR (2000) Mechanisms of cannabinoid inhibition of $GABA_A$ synaptic transmission in the hippocampus. J Neurosci 20:2470–2479.

Huang L, Keyser BM, Tagmose TM, Hansen JB, Taylor JT, Zhuang H, Zhang M, Ragsdale DS, Li M (2004) NNC 55-0396 [(1S,2S)-2-(2-(N-[(3-benzimidazol-2-yl)propyl]-N-methylamino)ethyl)-6-fluoro-1,2,3,4-tetrahydro-1-isopropyl-2-naphtyl cyclopropanecarboxylate dihydro

chloride]: a new selective inhibitor of T-type calcium channels. J Pharmacol Exp Ther 309:193–199.
Jensen K, Mody I (2001) L-type Ca^{2+} channel-mediated short-term plasticity of GABAergic synapses. Nat Neurosci 4:975–976.
Jonas P, Major G, Sakmann B (1993) Quantal components of unitary EPSCs at the mossy fibre synapse on CA3 pyramidal cells of rat hippocampus. J Physiol 472:615–663.
Jung MW, McNaughton BL (1993) Spatial selectivity of unit activity in the hippocampal granular layer. Hippocampus 3:165–182.
Kaneko A, Tachibana M (1986) Blocking effects of cobalt and related ions on the gamma-aminobutyric acid-induced current in turtle retinal cones. J Physiol 373:463–479.
Katona I, Sperlágh B, Sík A, Käfalvi A, Vizi ES, Mackie K, Freund TF (1999) Presynaptically located CB1 cannabinoid receptors regulate GABA release from axon terminals of specific hippocampal interneurons. J Neurosci 19:4544–4558.
Kerr AM, Reisinger E, Jonas P (2008) Differential dependence of phasic transmitter release on synaptotagmin 1 at GABAergic and glutamatergic hippocampal synapses. Proc Natl Acad Sci U S A 105:15581–15586.
Kim MH, Korogod N, Schneggenburger R, Ho WK, Lee SH (2005) Interplay between Na^{+}/Ca^{2+} exchangers and mitochondria in Ca^{2+} clearance at the calyx of Held. J Neurosci 25:6057–6065.
Kraushaar U, Jonas P (2000) Efficacy and stability of quantal GABA release at a hippocampal interneuron-principal neuron synapse. J Neurosci 20:5594–5607.
Leutgeb JK, Leutgeb S, Moser MB, Moser EI (2007) Pattern separation in the dentate gyrus and CA3 of the hippocampus. Science 315:961–966.
Li L, Bischofberger J, Jonas P (2007) Differential gating and recruitment of P/Q-, N-, and R-type Ca^{2+} channels in hippocampal mossy fiber boutons. J Neurosci 27:13420–13429.
Llano I, Gerschenfeld HM (1993) Inhibitory synaptic currents in stellate cells of rat cerebellar slices. J Physiol 468:177–200.
Llano I, González J, Caputo C, Lai FA, Blayney LM, Tan YP, Marty A (2000) Presynaptic calcium stores underlie large-amplitude miniature IPSCs and spontaneous calcium transients. Nat Neurosci 3:1256–1265.
Lou X, Scheuss V, Schneggenburger R (2005) Allosteric modulation of the presynaptic Ca^{2+} sensor for vesicle fusion. Nature 435:497–501.
Matveev V, Zucker RS, Sherman A (2004) Facilitation through buffer saturation: constraints on endogenous buffering properties. Biophys J 86:2691–2709.
Mayer ML, Vyklicky L Jr (1989) The action of zinc on synaptic transmission and neuronal excitability in cultures of mouse hippocampus. J Physiol 415:351–365.
McBain CJ, Fisahn A (2001) Interneurons unbound. Nat Rev Neurosci 2:11–23.
McKinney RA, Capogna M, Dürr R, Gähwiler BH, Thompson SM (1999) Miniature synaptic events maintain dendritic spines via AMPA receptor activation. Nat Neurosci 2:44–49.
Meinrenken CJ, Borst JGG, Sakmann B (2002) Calcium secretion coupling at calyx of Held governed by nonuniform channel-vesicle topography. J Neurosci 22:1648–1667.
Mitchell SJ, Silver RA (2003) Shunting inhibition modulates neuronal gain during synaptic excitation. Neuron 38:433–445.
Neher E (1998) Usefulness and limitations of linear approximations to the understanding of Ca^{++} signals. Cell Calcium 24:345–357.
Neher E, Sakaba T (2008) Multiple roles of calcium ions in the regulation of neurotransmitter release. Neuron 59:861–872.
Newcomb R, Szoke B, Palma A, Wang G, Chen X, Hopkins W, Cong R, Miller J, Urge L, Tarczy-Hornoch K, Loo JA, Dooley DJ, Nadasdi L, Tsien RW, Lemos J, Miljanich G (1998) Selective peptide antagonist of the class E calcium channel from the venom of the tarantula *Hysterocrates gigas*. Biochemistry 37:15353–15362.
Overstreet Wadiche L, Bromberg DA, Bensen AL, Westbrook GL (2005) GABAergic signaling to newborn neurons in dentate gyrus. J Neurophysiol 94:4528–4532.
Pang ZP, Bacaj T, Yang X, Zhou P, Xu W, Südhof TC (2011) Doc2 supports spontaneous synaptic transmission by a Ca^{2+}-independent mechanism. Neuron 70:244–251.
Pitler TA, Alger BE (1994) Depolarization-induced suppression of GABAergic inhibition in rat hippocampal pyramidal cells: G protein involvement in a presynaptic mechanism. Neuron 13:1447–1455.
Poncer JC, McKinney RA, Gähwiler BH, Thompson SM (1997) Either N- or P-type calcium channels mediate GABA release at distinct hippocampal inhibitory synapses. Neuron 18:463–472.
Randall A, Tsien RW (1995) Pharmacological dissection of multiple types of Ca^{2+} channel currents in rat cerebellar granule neurons. J Neurosci 15:2995–3012.
Randall AD (1998) The molecular basis of voltage-gated Ca^{2+} channel diversity: is it time for T? J Membr Biol 161:207–213.
Ribrault C, Sekimoto K, Triller A (2011) From the stochasticity of molecular processes to the variability of synaptic transmission. Nat Rev Neurosci 12:375–387.
Scanziani M, Capogna M, Gähwiler BH, Thompson SM (1992) Presynaptic inhibition of miniature excitatory synaptic currents by baclofen and adenosine in the hippocampus. Neuron 9:919–927.
Soltesz I, Smetters DK, Mody I (1995) Tonic inhibition originates from synapses close to the soma. Neuron 14:1273–1283.
Stanley EF (1997) The calcium channel and the organization of the presynaptic transmitter release face. Trends Neurosci 20:404–409.
Sun J, Pang ZP, Qin D, Fahim AT, Adachi R, Südhof TC (2007) A dual-Ca^{2+}-sensor model for neurotransmitter release in a central synapse. Nature 450:676–682.
Sutton MA, Ito HT, Cressy P, Kempf C, Woo JC, Schuman EM (2006) Miniature neurotransmission stabilizes synaptic function via tonic suppression of local dendritic protein synthesis. Cell 125:785–799.
Vyleta NP, Smith SM (2011) Spontaneous glutamate release is independent of calcium influx and tonically activated by the calcium-sensing receptor. J Neurosci 31:4593–4606.
Westenbroek RE, Ahlijanian MK, Catterall WA (1990) Clustering of L-type Ca^{2+} channels at the base of major dendrites in hippocampal pyramidal neurons. Nature 347:281–284.
Wilson RI, Kunos G, Nicoll RA (2001) Presynaptic specificity of endocannabinoid signaling in the hippocampus. Neuron 31:453–462.
Xu J, Pang ZP, Shin OH, Südhof TC (2009) Synaptotagmin-1 functions as a Ca^{2+} sensor for spontaneous release. Nat Neurosci 12:759–766.
Yamasaki M, Hashimoto K, Kano M (2006) Miniature synaptic events elicited by presynaptic Ca^{2+} rise are selectively suppressed by cannabinoid receptor activation in cerebellar Purkinje cells. J Neurosci 26:86–95.
Yao J, Gaffaney JD, Kwon SE, Chapman ER (2011) Doc2 is a Ca^{2+} sensor required for asynchronous neurotransmitter release. Cell 147:666–677.